

# Development of Nanoparticle-Stabilized Foams To Improve Performance of Water-less Hydraulic Fracturing

CONTRACT NO. DE- FE0013723  
**QUARTERLY PROGRESS REPORT**  
**Reporting Period: 1 Jan 14 – 31 Mar 14**  
**Project Period: 1 Oct 13 – 30 Sep 16**

Prepared by *Steven Bryant*

**Steven L. Bryant (PI) and Chun Huh (co-PI)**  
Department of Petroleum and Geosystems Engineering  
The University of Texas at Austin  
1 University Station C0300  
Austin, TX 78712-0228  
Phone: (512) 471 3250  
Email: [steven\\_bryant@mail.utexas.edu](mailto:steven_bryant@mail.utexas.edu) and [chunhuh@mail.utexas.edu](mailto:chunhuh@mail.utexas.edu)  
DUNS: 170230239

and

**Keith P. Johnston (co-PI)**  
Department of Chemical Engineering  
The University of Texas at Austin  
1 University Station C0300  
Austin, TX 78712-0228  
Phone: (512) 471 4617  
Email: [johnston@che.utexas.edu](mailto:johnston@che.utexas.edu)

Prepared for

**U.S. Department of Energy - NETL**  
3610 Collins Ferry Road  
P.O. Box 880  
Morgantown, WV 26508

Acknowledgment: "This material is based upon work supported by the Department of Energy under Award Number DE-DE- FE0013723."

Disclaimer: "This report was prepared as an account of work sponsored by an agency of the United States Government. Neither the United States Government nor any agency thereof, nor any of their employees, makes any warranty, express or implied, or assumes any legal liability or responsibility for the accuracy, completeness, or usefulness of any information, apparatus, product, or process disclosed, or represents that its use would not infringe privately owned rights. Reference herein to any specific commercial product, process, or service by trade name, trademark, manufacturer, or otherwise does not necessarily constitute or imply its endorsement, recommendation, or favoring by the United States Government or any agency thereof. The views and opinions of authors expressed herein do not necessarily state or reflect those of the United States Government or any agency thereof."

## Executive summary

One of the objectives of the project is to develop nanoparticle-stabilized foams that have a very low water content (< 25 vol. %), yet exhibit high apparent viscosity with robust stability, so that they can be used as nearly water-less fracturing fluids. During this quarter we focused on two tasks: (i) examining the effects of polymer addition upon increasing the foam quality (reducing water content) without breaking the foam, and (ii) the development of a model that defines the conditions for foam breakage in the fracture when the post-frac flow-back operation is performed.

Building on our earlier finding that the foams with high apparent viscosity can be generated by capitalizing on synergy between the nanoparticles and a very low concentration of betaine surfactant, we were able to generate stable 90% quality CO<sub>2</sub>-in-water foams with apparent viscosities as high as 50 cp, with addition of 0.1 % of partially hydrolyzed polyacrylamide (HPAM) polymer.

Concurrent to the development of the nanoparticle-stabilized CO<sub>2</sub> foam transport model, carried out by another DOE NETL project (“Use of Engineered Nanoparticle-Stabilized CO<sub>2</sub> Foams to Improve Volumetric Sweep of CO<sub>2</sub> EOR Processes”), the foundation for a mechanistic foam dynamics model has been defined. The model is specifically for the case of nanoparticle-stabilized foams, the mechanisms of which need not be the same as traditional surfactant-stabilized foams. Moreover the aim of the model is to quantify the conditions for foam breakage in the fracture when the post-frac flow-back operation is performed, so that the foam does not interfere with the subsequent hydrocarbon production. Our hypothesis is that nanoparticle-stabilized foams can be tuned or engineered to break at target pressures, and that this ability can be exploited to provide frac fluids that clean up more effectively.

## Activities During This Reporting Period

### I. Effects of Polymer on Increasing Foam Quality

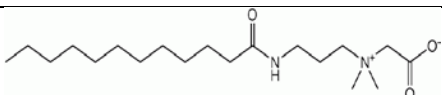
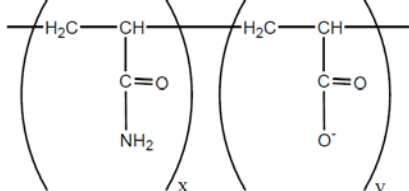
High viscosity carbon dioxide-in-water C/W foams were generated by mixtures of partially hydrolyzed acrylamide polymers, surface-modified silica nanoparticles, and betaine surfactants in the aqueous phase. Most importantly, with the addition of 0.1 % HPAM it was possible to generate stable foams of 90% quality (i.e. only 10% water by volume). The apparent viscosity of foams generated with aqueous phases containing HPAM reached 68 cP measured in the capillary tube.

The effect of varying the phase ratio of injected fluids on foam viscosity was investigated. This was motivated by the potential benefit of following the injection of a foam slug by a pure CO<sub>2</sub> slug to break the foam. After the foam generation process (co-injection of CO<sub>2</sub> and aqueous phase at desired phase ratio through a bead pack) reached steady state, the injection of the aqueous phase was stopped, and the rate of CO<sub>2</sub> injection was increased to maintain a constant total flow rate. Importantly, when the foam quality was initially high (0.9), the foam viscosity decreased very rapidly (in much less than 1 pore volume), indicating a rapid destabilization which did not require a large volume of CO<sub>2</sub> to trigger. This feature could be very useful in developing low-water frac fluids that clean up easily.

#### I.1. Experimental

**Materials.** Surface-modified colloidal silica nanoparticles (EOR-5XS, Lot No. LB130204, Nissan Chemical America Corporation) were received as a 20 % w/v aqueous dispersion. The nanoparticles have a proprietary, covalent surface modification as provided by the manufacturer. Lauramidopropyl betaine (LAPB) (Mackam DAB-ULS, Lot UP1J13X04, 35 % w/v) was a gift from Rhodia and was used as received. Flopaam 3630S was received from SNF Floerger and used as received. The Flopaam 3630S is a partially hydrolyzed polyacrylamide polymer and has a molecular weight of 20 M Dalton. Potassium Chloride (KCl) was obtained from Fisher Scientific and used as received.

**Table I-1.** Chemical structure of LAPB surfactant and HPAM polymer.

Chemical	Structure
LAPB	
HPAM	

**Polymer hydration.** Flopaam 3630S is received as powder samples. Proper hydration of powdered polymers at different concentrations can be obtained by the following procedure. Polymer powder was added slowly to a low salinity brine solution (1 % KCl) on a stir plate at 400-600 rpm using a cross shaped magnetic stir bar. With the addition of polymer powders, the solution became highly viscous and the stir bar was slowed to 100-200 rpm. The solutions became transparent after 1-2 h and the slow stirring was continued for a minimum of 16 hrs before use to allow for full hydration of the polymers.

**Polymer filtration.** Filtration tests are conducted to ensure that the polymer solution can pass through porous media (foam generator and proppant bed). Briefly, 250 mL polymer solutions were loaded into in a 90 mm filter press cell with a 1.2 micron Millipore cellulose filter (part # RAWP 09025) and filtered under 15 psi Ar. The filtration ratio is calculated (equation 1) based on the time when 60, 80, 180 and 200 mL of fluids have been filtered and polymer solutions with filtration ratio below 1.2 were used for foam studies.

$$FR = \frac{t_{200\text{ mL}} - t_{180\text{ mL}}}{t_{80\text{ mL}} - t_{60\text{ mL}}} \quad (\text{I-1})$$

**Compatibility of polymers, surfactants and nanoparticles.** All the chemicals used for generating and stabilizing CO<sub>2</sub> foams must be compatible in aqueous phase. Aqueous solutions of polymers, surfactants, nanoparticles and salts were visually observed for 2 weeks at 50°C. Clear solution was obtained and no precipitation or phase separation was observed.

**Foam generation and characterization.** Foams were generated at 2800 psi, 50°C and the apparent viscosities were measured in the same manner as reported in Y1Q1 report.

## **I.2. High viscosity C/W foams generated by mixtures of partially hydrolyzed acrylamide polymers, surface-modified silica nanoparticles and betaine surfactants**

The apparent viscosity of C/W foams of different qualities generated with Flopaam 3630S acrylamide polymers (HPAM), surface-modified EOR-5XS nanoparticles (NPs) and LAPB in 2% KCl are shown in Figure 1. All the foams were generated at a superficial velocity of 200 ft/day. At foam quality (gas fraction) of 0.75, the mixture of NPs and LAPB surfactants generated strong foam of 27 cP. When 0.02 % HPAM was added, the apparent viscosity was unchanged. However, addition of higher concentrations of HPAM led to dramatic increases of apparent viscosity of foam. With the addition of 0.1 % HPAM, the apparent viscosity of foam reached 68 cP. The bulk foam viscosity  $\mu$ , according to Princen's model (equation I-2), is a strong function of foam quality ( $\phi$ ), the external phase viscosity ( $\mu_e$ ), interfacial tension ( $\sigma$ ), shear rate ( $\dot{\gamma}$ ) and mean bubble size ( $R_{32}$ ). At constant superficial velocities, the increasing

viscosity of the aqueous phase (increased  $\mu_e$ ) likely led to smaller bubble sizes and aqueous lamellae which resist drainage, and thus to an increase of the apparent viscosity of foams. Interestingly, without the presence of 1 % nanoparticles, HPAM and LAPM mixtures alone failed to generate strong foams. Presumably, due to the low concentration of 0.01 % LAPB used, the amount of surfactant was not high enough to stabilize lamellae and thus only weak foam was observed.

$$\mu = \frac{\tau_0}{\dot{\gamma}} + C(\phi)\mu_e \left( \frac{\sigma}{\mu_e \dot{\gamma} R_{32}} \right)^{\frac{1}{3}} \quad (\text{I-2})$$

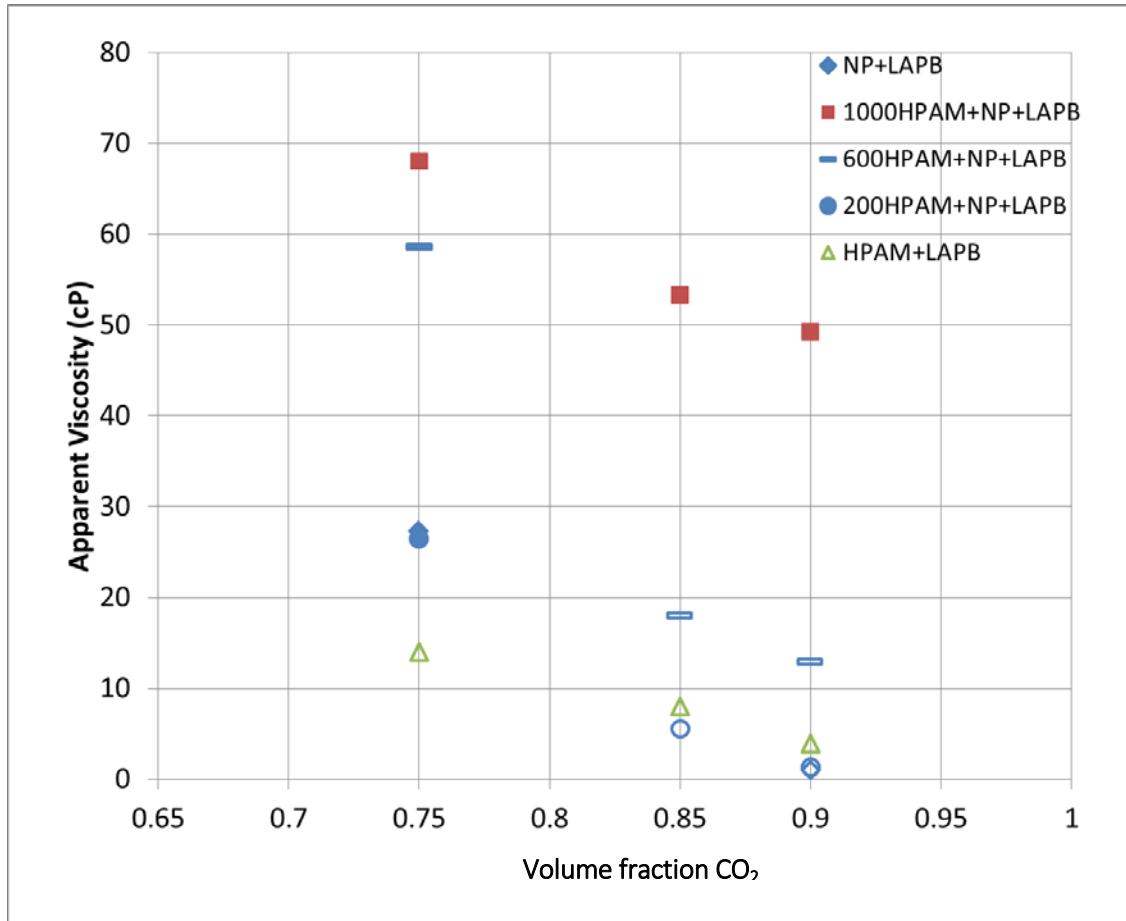
With an injected CO<sub>2</sub>/water phase ratio of 0.9, no foam was observed when using mixtures of NPs and LAPB (Figure I-1). Even with 0.02 % or 0.06 % HPAM added to the aqueous phase, only weak foam was observed. However, strong foam with apparent viscosity of ~50 cP was observed with the addition of 0.1% HPAM. The same trend was also observed at 0.85 phase ratio, where strong foams were observed when 0.1% HPAM was added to the aqueous phase. This is an extraordinary degree of synergy between the aqueous phase additives, and to our knowledge this is the first demonstration of this phenomenon.

The nanoparticle/surfactant/polymer synergy has potentially profound implications for frac fluid design because the viscosities of the resulting foams are quite large. It is important then to understand the mechanisms at work in this system. To generate strong foam, the applied shear (viscous) forces must overcome the interfacial forces. For traditional foams in porous media, there exists a minimum pressure gradient across the porous medium to displace lamellae from the pore throats and mobilize them (equation I-3).

$$\begin{aligned} \nabla p^{min} & \quad (\text{I-3}) \\ & = \frac{8f_{nw}\sigma}{L} \sqrt{\frac{4\phi^3}{150k(1-\phi)^2}} \end{aligned}$$

where  $f_{nw}$  is the fractional flow of the non-wetting phase (gas phase),  $\sigma$  is the interfacial tension,  $k$  is the permeability of the permeable media, and  $\phi$  is the porosity. (The term beneath the radical is a measure of reciprocal grain size in the porous medium.) The minimum pressure gradient depends on the fractional flow of the non-wetting phase, in this case, the gas. The effect of foam quality may also extend to the possible difference of interfacial tension at different phase ratios since the amount of surfactant at 0.9 CO<sub>2</sub> phase volume fraction is only 40 % of that at 0.75 CO<sub>2</sub>-phase volume fraction due to the smaller volume of the aqueous phase that is present. Thus an even higher minimum pressure gradient may be required for generation of such high quality foams. These considerations suggest that the mixtures of NPs and LAPB do not produce stable foam at a 0.9 CO<sub>2</sub> phase volume fraction because the applied pressure gradient is not large enough to mobilize the lamellae. At constant superficial velocities, however, increasing the

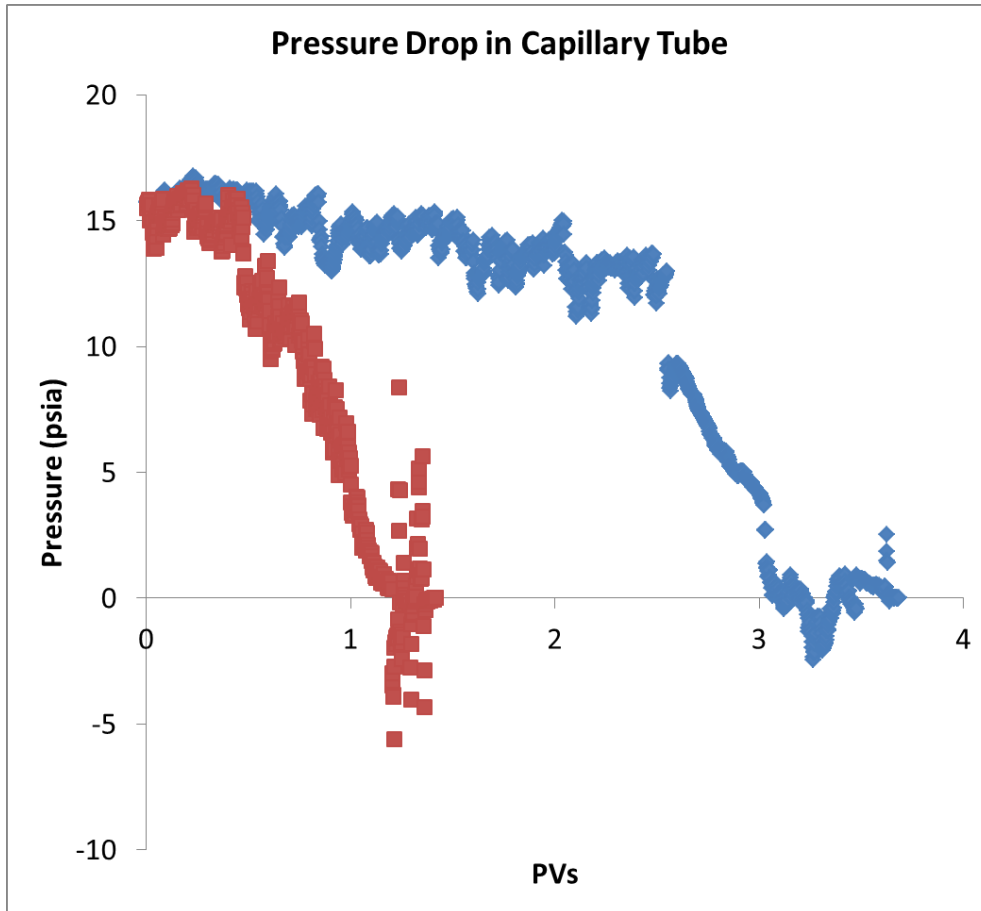
viscosity of the aqueous phase will necessarily require a higher applied pressure gradient. At a temperature of 50°C, the viscosity of water is only ~0.5 cP, whereas 0.1 % HPAM solution has a viscosity of ~5 cP. We hypothesize that with the high concentration of 0.1 % HPAM added to NPs and LAPB mixtures, the applied pressure gradient exceeded the minimum pressure gradient for lamella mobilization and thus strong foam was generated.



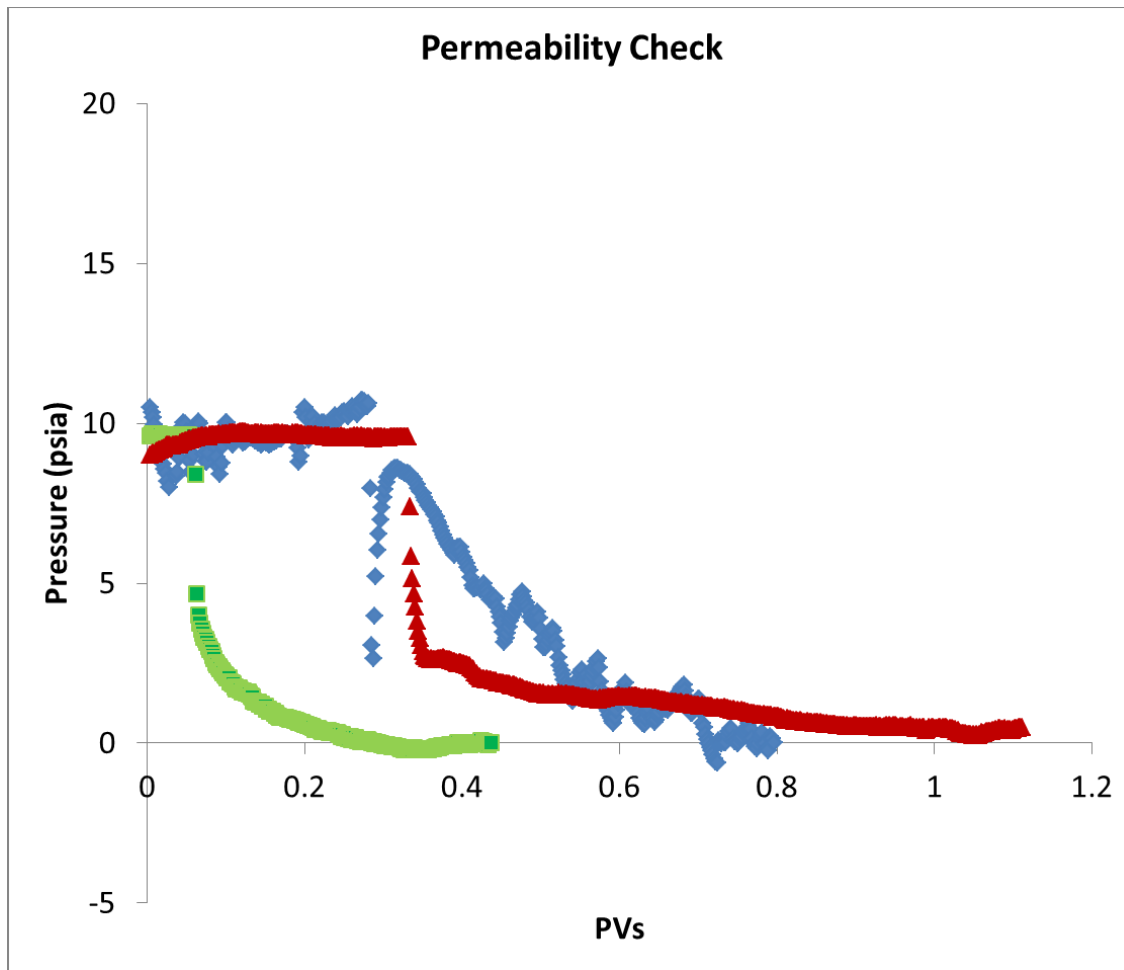
**Figure I-1.** Apparent viscosity of C/W foams generated at a superficial velocity of 200 ft/day with Flopam 3630S acrylamide polymers (HPAM), surface-modified EOR-5XS nanoparticles (NPs) and LAPB in 2% KCl. The concentration of HPAM was varied from 0, 200, 600 and 1000 ppm (0, 0.02, 0.06, and 0.1%), the concentration for nanoparticles and LAPB was fixed at 1 % and 0.01%, respectively. Open symbols represent no foam or weak foam, solid symbols represents strong foam. The addition of 1000 ppm HPAM enabled a viscous foam of quality 0.9 to be generated; at smaller concentrations of HPAM no foam was generated. This is consistent with the idea of a critical pressure gradient for foam generation (see text).

Figure I-2 shows the pressure drop in capillary tube (downstream of the foam-generating beadpack) of two replicate experiments, generating 0.9 quality foam using formulation of 1 % NPs, 0.01% LAPB, 0.1% HPAM in 2 % brine solution at 2800 psi and 50°C. The pressure drop histories for the two separate runs agree well. The permeability of the foam-generating beadpack

was measured after each run by recording the pressure drop across the beadpack with a known flowrate of DI water and compared with the permeability of the beadpack before the foam generation experiments. As shown in Figure 3, the pressure drop of the beadpack to DI water flooding (green line) was ~10 psi at a flow rate of 10 mL/min. After each run of 0.9 quality foam generation with 1 % NPs, 0.01% LAPB, 0.1% HPAM in 2 % brine solution at 2800 psi, 50 C, the beadpack was washed with water and the pressure drop profile was recorded, as presented in Figure 3 (red and blue line). The pressure drop remained the same, indicating the permeability of the beadpack was unchanged after foam flooding.



**Figure I-2.** Pressure drop (raw data) in capillary tube of two foam generation experiments conducted in a beadpack upstream of the capillary tube at a superficial velocity of 200 ft/day at 2800 psi, 50°C and at a 0.9 quality, with the aqueous phase formulation of 1 % NPs, 0.01% LAPB, 0.1% HPAM in 2 % brine solution.



**Figure I-3.** Pressure drop for permeability measurements before and after foam generation. Green line represents the pressure drop of freshly prepared beadpack with respect to DI water flooding. After foam generation, the beadpack was washed with water. Red line and blue line are two reproducible measurements representing the pressure drop across the beadpack after the foam generation experiments.

### I.3. Foam breakage by drying

Drying of the foam by increasing CO<sub>2</sub> volume fraction was explored as a means to break the viscous foam. Initially, both CO<sub>2</sub> and an aqueous phase containing chemical formulations were injected until a steady state pressure drop was obtained. Then, the aqueous phase flow was stopped, and the CO<sub>2</sub> phase flow was increased to maintain a constant total flow rate (and therefore constant shear rate in the beadpack and capillary tube). The change in injection profile is marked as “shut in” in Figure I-4 and Figure I-5. By increasing the CO<sub>2</sub> flow rate while shut in the aqueous pump, the foam in the beadpack will be slowly displaced by CO<sub>2</sub>. This displacement process leads to a monotonic increase in average foam quality (phase ratio) in the



beadpack and capillary tube, and thus a change of the foam apparent viscosity. The pressure drop response due to such change was recorded.

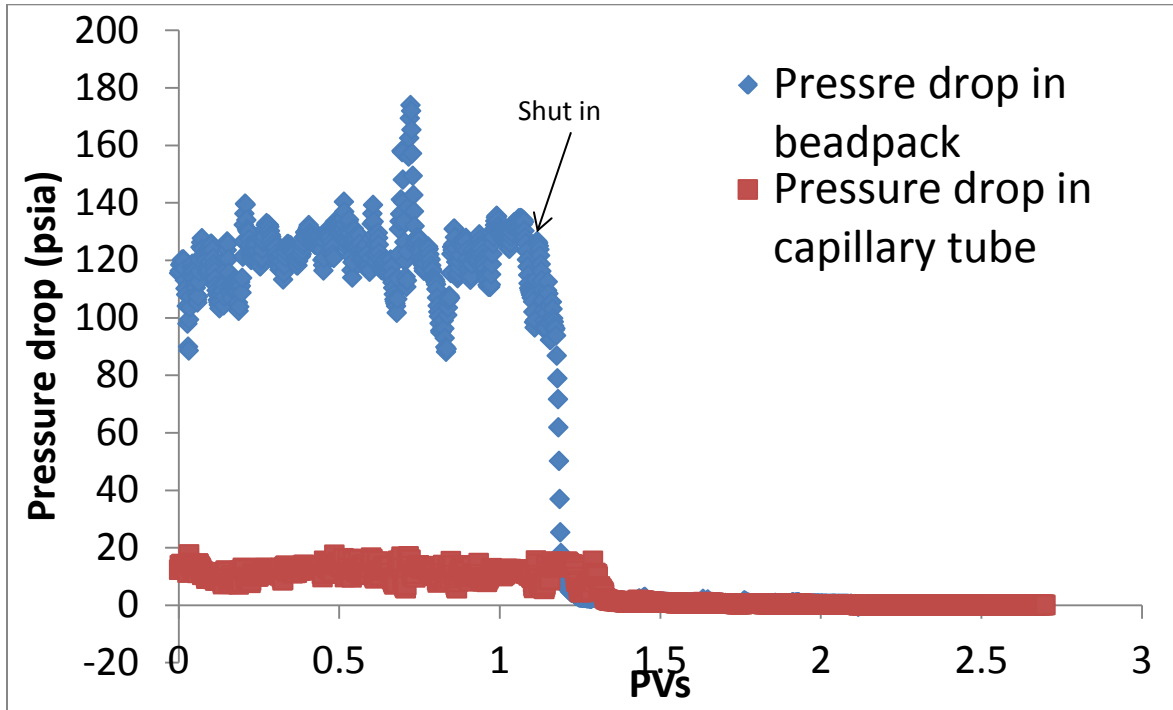


**Figure I-4.** Pressure drop history across the beadpack (blue) and capillary tube (red) during drying of foam by altering injection phase volume fraction. Foam with 0.9 quality was generated steadily for 1.1 PV with 1 % NPs, 0.01% LAPB, 0.1% HPAM in 2 % brine at 2800 psi, 50°C, and total flow rate of 0.5 mL/min (shear rate  $\sim 200 \text{ s}^{-1}$  in capillary tube, shear rate  $\sim 400 \text{ s}^{-1}$  and Darcy velocity  $\sim 200 \text{ ft/day}$  in beadpack). At the point marked “shut in” the aqueous phase injection was halted and the  $\text{CO}_2$  volumetric injection rate was increased to maintain constant shear rate in the beadpack.

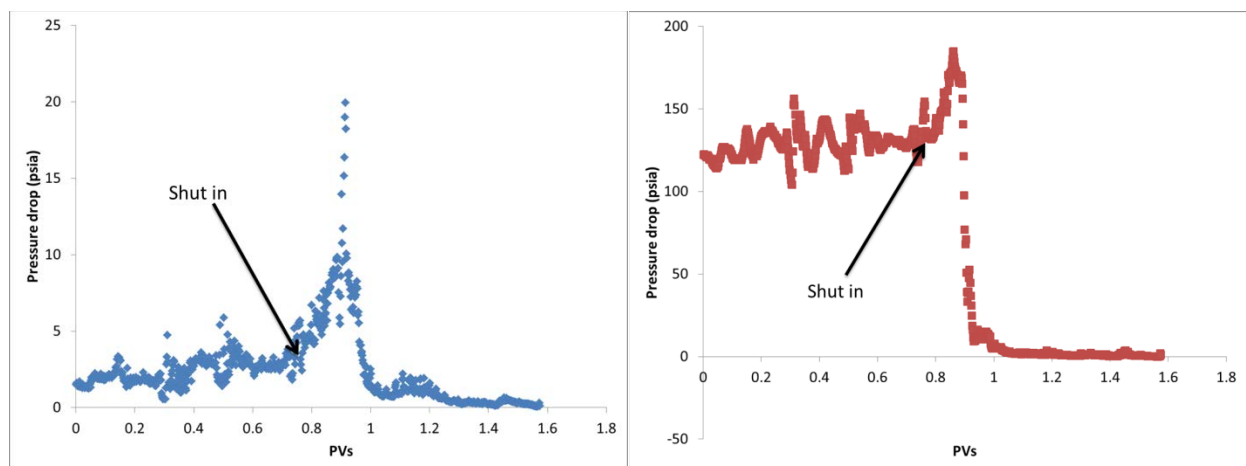


**Figure I-5.** Pressure drop history across the capillary tube (left) and beadpack (right) during drying of foam by altering injection phase volume fraction. Foam with 0.5 quality was generated steadily for 0.75 PV with 1 % NPs, 0.01% LAPB, 0.1% HPAM in 2 % brine at 2800 psi, 50°C, and total flow rate of 0.5 mL/min (shear rate  $\sim 200 \text{ s}^{-1}$  in capillary tube, shear rate  $\sim 400 \text{ s}^{-1}$  and Darcy velocity  $\sim 200 \text{ ft/day}$  in beadpack). At the point marked “shut in”, the aqueous phase injection was halted and the  $\text{CO}_2$  phase flow rate increased to keep the shear rate constant.

Drying of foams stabilized with 1 % NPs, 0.01% LAPB and 0.1% HPAM in 2 % brine was investigated. The pressure drop data of foam started at 0.9 quality was shown in Figure I-4. The steady state pressure drop is  $\sim 120 \text{ psia}$  in beadpack, and  $\sim 15 \text{ psia}$  in capillary tube, was consistent with the results shown in Figure 2. After shut-in of water pump and switch to pure  $\text{CO}_2$  at 1.1 PVs, a rapid decrease of pressure drop to  $< 2 \text{ psia}$  was observed. It is likely that at high foam quality of 0.9,  $\text{CO}_2$  rapidly percolated through the foam after the aqueous phase flow was stopped, causing the initially gas-discontinuous foam became gas-continuous. We hypothesize that this phenomena lead to the observed rapid decrease of pressure drop. Similarly, drying of foam with initial quality of 0.5 was investigated. Figure I-5a shows the pressure drop history in capillary tube. At 0.5 quality, only weak foam was observed in the view cell, in agreement with the low steady state pressure drop of  $\sim 2 \text{ psia}$  in the capillary tube. Interestingly, after switching to pure  $\text{CO}_2$ , the pressure drop first increased to  $\sim 20 \text{ psia}$  and then decreased gradually to  $< 2 \text{ psia}$ . A similar trend of pressure drop was also observed in beadpack. We hypothesize that this phenomenon is due to the changing average quality of foam. The initial quality of 0.5 is below the optimum quality of 0.75, where highest viscosity foam was produced. As the foam displaced by pure  $\text{CO}_2$ , the average foam quality increases as a result. The viscosity first increases, and then decreases as the average foam quality goes above the optimum. Importantly, when the foam quality was initially high (0.9), the foam viscosity decrease occurred

over much less than 1 pore volume, indicating a rapid destabilization which did not require a large volume of CO<sub>2</sub> to trigger.

## **II. Modeling of Post-Frac Flowback of Low Water-Content Foam**

### **II.1. Introduction**

In conventional frac jobs water and thickeners like guar gum are used to move and place sands into the fractures. During a frac job high viscosity of frac fluids are advantageous for conveying proppant. Viscosity is a disadvantage during flowback the fluid may help produce proppant back into the well and may be left within the propped fracture as less viscous gas is produced from the matrix and flows preferentially through only a portion of the proppant pack. This reduces productivity index. Foams show high viscosity and, more interestingly, by changing operating conditions such as pressure they may collapse and lose their viscosity. Thus they have the advantages of traditional viscosified fluids without the disadvantages.

Here we are developing models to determine optimum pressure profiles to keep foams stable during fracturing and to break them during flowback. Our previous studies on nanoparticle stabilized foams suggested them as promising fluids, since their stability is sensitive to pressure and upon pressure reduction they collapse immediately. In the following we develop a model to simulate behavior of foam during flow back and determine foam collapse profile inside the fracture.

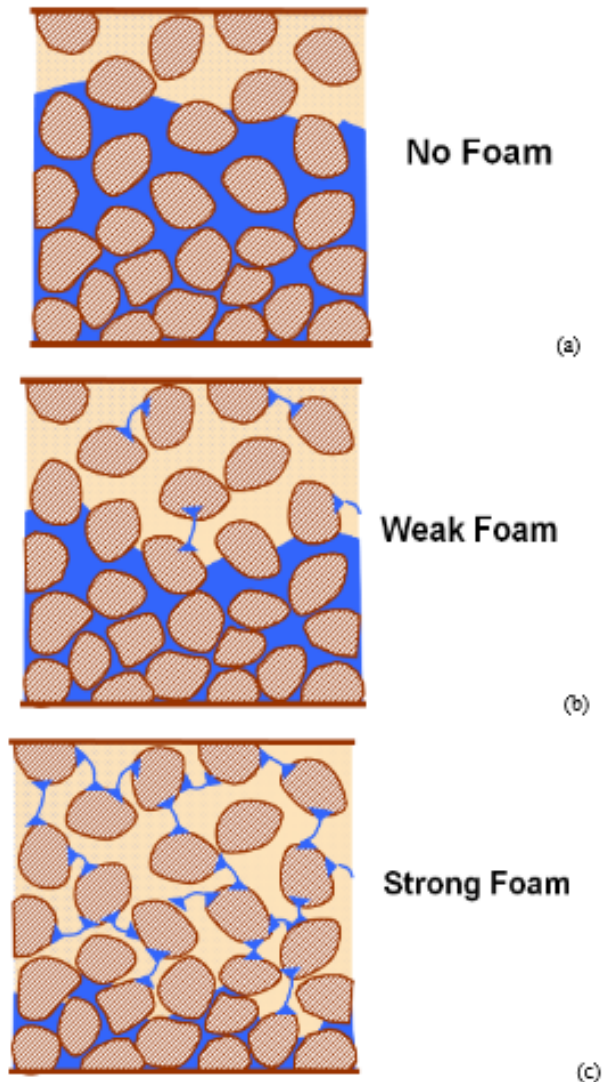


**Figure II-1:** Foam flow in porous media, (a) gas-liquid two phase segregated flow, (b) weak foam, (c) strong foam. (Dholkawala (2006))

## II.2. Foam in porous media

Figure II-1 shows schematic of foam structures in porous media. In the simplest case gas and liquid phases flow segregated into the porous media. When enough surfactants are available gas and liquid can form lamella films and stable foams inside porous media. Foams themselves are categorized as weak and strong. With weak foams the number of lamella films per unit volume of the porous media is not significant so their physical properties are more similar to the segregated flow. When lamella films form with high density then viscosity of the foams significantly increases. In this case the foam is considered as strong foam.

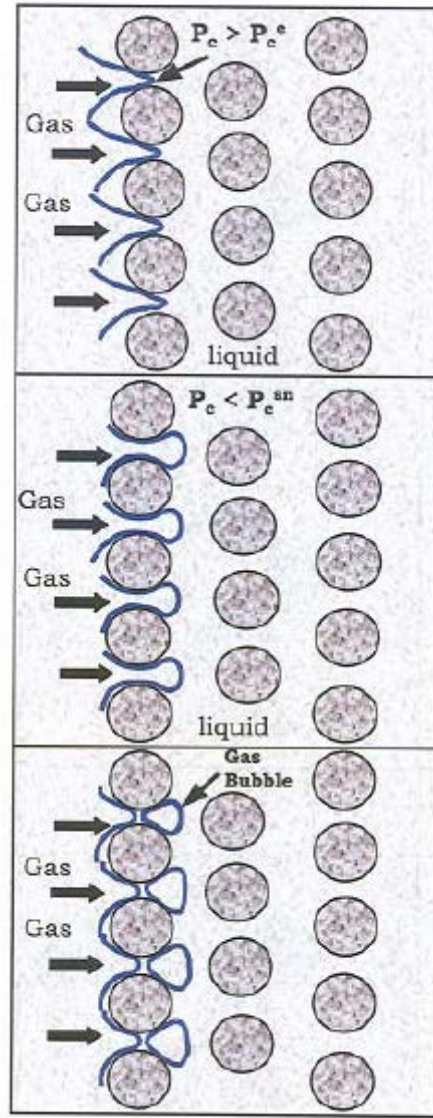


**Figure II-2:** Lamella creation mechanism, Snap off. (Dholkawala, 2006)

### II.3. Disjoining Pressure

When capillary pressure and disjoining pressures are equal then the lamella is stable

$$\frac{2\sigma}{r} = P_d(h)$$

with  $P_d$  as disjoining pressure and  $h$  is thickness of lamella. Disjoining pressure is mainly result of intermolecular and particle interactions like van der Waals attractions and electrostatic and steric repulsions. If the film thickness drops below a critical distance then attractive forces become dominant and the liquid film between two bubbles disappear resulting in the coalescence of the bubbles. When the lamella film becomes thinner, a maximum repulsive force mostly due

to electrostatic repulsion and steric hindrance appears, and at this maximum the disjoining pressure reaches to its highest value.

If the capillary pressure stays below the critical capillary pressure, stable lamella films and bubbles can form. In porous media foam generation is mainly attributed to the snap off process, when the liquid is pressed and pushed between solid rock grains. If the capillary pressure of the liquid is lower than the critical pressure (maximum disjoining pressure) then stable lamella films can form. Figure II-2 shows schematic of foam creation process during snap off process.

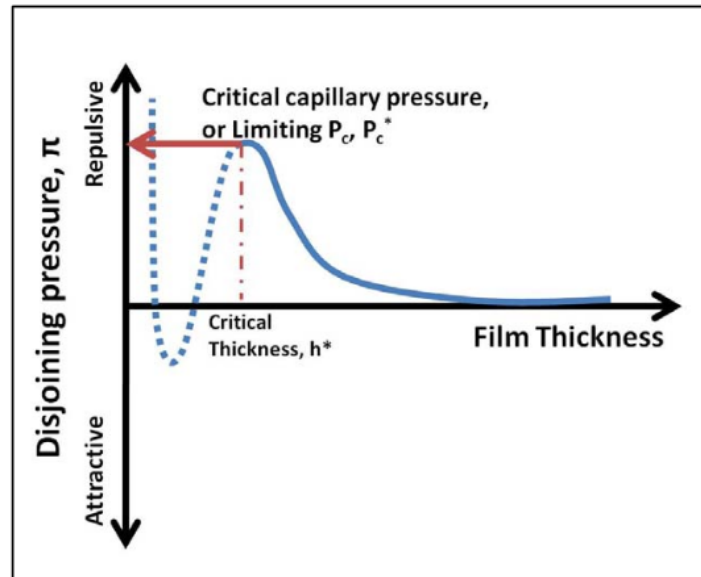


**Figure II-3:** Profile of disjoining pressure as a function of film thickness. At  $h_{max}$  disjoining pressure reaches its critical value,  $P_c^*$ . (Aronson et al., 1994)

Figure II-3 shows the profile of disjoining pressure as a function of liquid film thickness. Long range attractive van der Waals forces that destabilize film stability appear roughly at 10 nm while they become balanced by repulsive electrostatic and steric interactions at about 5 nm, where the critical capillary pressure appears. Once the thickness falls below the critical value the attractive forces become dominant and film becomes unstable.

Core flood experiments done by Alvarez et al with different surfactants and on a wide range of experimental conditions surfactant concentrations and porous matrices showed that for wet foams (low quality) the pressure drop is almost independent of liquid velocity whereas for high quality foams the pressure drop is independent of gas velocity. There is a certain foam quality at which the flow regime suddenly switches from one type to another. It was shown that the high quality foam was controlled by bubble coalescence near capillary pressure whereas bubble trapping and mobilization is dominant for low quality foam.

Further experiments relate the sudden change of the flow regime in the porous media to the catastrophic foam destruction inside the matrix. Catastrophic behavior of foams appears in a wide range of operating conditions including different surfactants, gas bubbles and porous media. These findings are all consistent with the theory of foam generation which explains sudden change from weak foam to strong foam upon increasing shear rates at a constant foam quality.

#### II.4. Fractional flow model for fluid transport in porous media

Inside porous media the shape of foam bubbles depends on the foam quality. If the foam quality is low the bubbles can keep their spherical shapes. In this case previous calculations are valid and upon pressure reduction the bubbles expand and interbubble gas diffusion accelerates. When foam quality increases then the gas bubbles would be segments of pores inside the porous media separated by lamella. So there is no correlation between their local curvature and their volume. In this case the previous equations would not be valid. To simulate behavior of foams inside proppant and porous matrix we employ fractional flow model. Mass balance of two immiscible phases in the absence of adsorption is given by (Lake, 1989)

$$\frac{\partial}{\partial t}(\phi \rho_j S_j) + \nabla \cdot (\rho_j u_j) = G$$

The index  $j$  is either liquid or gas phase. For a one dimensional incompressible flow with no source or sink, the equation can be simplified to

$$\frac{\partial}{\partial t}(S_j) + \frac{u_t}{\phi} \frac{\partial}{\partial x}(f_j) = 0$$

$S$  is saturation,  $f$  is fractional flow,  $\phi$  is porosity,  $u_j$  is superficial velocity,  $u_t$  is total injection velocity and  $G$  is source or sink term. Equations for liquid and gas phases are related by saturations and fractional flow (both sum to unity), therefore only one of them is independent.

It has been shown that foam formation only affects gas relative permeability while water relative permeability is intact. The relative permeability of water and gas are empirically defined as functions of saturations and various critical or residual saturations by

$$k_{rw} = 0.7888 \left( \frac{S_w - S_{wc}}{1 - S_{wc} - S_{gr}} \right)^{1.9575}$$

$$k_{rg}^0 = \left( \frac{1 - S_w - S_{gr}}{1 - S_{wc} - S_{gr}} \right)^{2.2868}$$

$$k_{rg}^f = \left( X_f \frac{1 - S_w - S_{gr}}{1 - S_{wc} - S_{gr}} \right)^{2.2868}$$

where  $S_{wc}$  and  $S_{gr}$  are connate water saturation and residual gas saturation.  $X_f$  is fraction of flowing gas which is related to the fraction of trapped gas via

$$X_f = 1 - X_t$$

Fraction of trapped gas is calculated via the following empirical model

$$X_t = X_{tmax} \left( \frac{\beta n_f}{1 + \beta n_f} \right)$$

$X_{tmax}$  and  $\beta$  are parameters of the models which are assumed constant. If the system is assumed to be at thermodynamic equilibrium then (Kam, et al. 2007)

$$n_f = \frac{C_g}{2C_c} \left( \frac{S_w - S_w^*}{S_w} \right)^n \left\{ erf \left( \frac{\nabla P - \nabla P_0}{\sqrt{2}} \right) - erf \left( \frac{-\nabla P_0}{\sqrt{2}} \right) \right\}$$

Water fractional flow is defined as

$$f_w = 1 - f_g = \frac{u_w}{u_t} = \left( 1 + \frac{k_{rg}/\mu_g}{k_{rw}/\mu_w} \right)^{-1}$$

$k_{rg}^0$  and  $k_{rg}^f$  are gas relative permeability in the absence and presence of foams. In the presence of foams gas viscosity is related to the foam viscosity as follows (Hirasaki and Lawson, 1985)

$$\mu_g^f = \mu_g^0 + \frac{C_f n_f}{\left( u_g / (\phi S_g X_f) \right)^{1/3}}$$

$\mu_g^0$  is gas viscosity in the absence of foam and  $C_f$  is a model parameter. Bubble population balance model is developed to predict foams texture as a function of velocity in the porous matrix as follows, (Falls et al. 1988)

$$\phi \frac{\partial}{\partial t} (S_g n_f) + \frac{\partial}{\partial x} (n_f u_g) = \phi S_g R$$

$n_f$  is foam texture (number of foams films unit gas volume,  $R$  is the net change of  $n_f$ . On the left hand side, first term is bubble accumulation and second term is bubble advection term. Using this equation we can mechanistically simulate the bubble population with time and space. If the water saturation falls below the limiting saturation ( $S_w < S_w^*$ ), foam films will no longer sustain which leads to  $n_f = 0$ . In addition, there is a maximum value for the foams texture,  $n_{fmax}$ ). If the calculated foam texture goes beyond this value it will be corrected to  $n_f = n_{fmax}$ . This is because



bubbles cannot be smaller than average poresize due to the diffusion, and minimum bubble size is equivalent to a maximum foam texture. The net rate of foam generation is equal to rate of generation minus rate of coalescence.

**Table II-1:** Physical properties of the foam system modeled in this study

Petrophysical Props		Foam props		Foam params	
k (m2)	$3.04 \cdot 10^{-11}$	$n_{fmax}$	$8 \cdot 10^{13}$	$\nabla P_0$ (psi/ft)	4.2
$\phi$	0.31	$S_w^*$	0.0585	n	0.28
$\mu_w$ (Pa.s)	0.001	$X_{tmax}$	0.8	m	2.4
$\mu_g^0$ (Pa.s)	0.00002	$\beta$	$5 \cdot 10^{-11}$	$C_g/C_c$	$3.6046 \cdot 10^{13}$
$S_{gr}$	0			$C_f$	$6.617 \cdot 10^{-14}$
$S_{wc}$	0.04				

## II.5. Problem formulation

Here we assume reservoir pressure ( $P_r$ ) at 4500 psi, frac treating pressure ( $P_f$ ) at 6000 psi and production or flowback pressure ( $P_p$ ) at 3500 psi. Figure II-4 shows a schematic view of a fracture in the formation. Here we assume a fracture as two vertical parallel planes. During fracing the size of a fracture is taken to be 100 by 100 meters by area and 1 cm width. When pressure is reduced to the reservoir pressure then the fracture will be reduced in size to 50 m by 50 m and about 1 mm width.

After the frac is pumped, pressure reduction allows backflow and removes fracking fluid from the cracks. This process can be divided into two parts. First part is reducing pressure from fracking pressure to the reservoir pressure. At this step volume of the fracture is changing. In addition since pressure of frac fluid is larger than the formation pressure, no gas will diffuse from the formation into the fracture and all discharge of the frac fluid is due to the reduction in the volume of the fracture. In addition, in this step we assume that permeability of the formation is so low that the frac fluid will not diffuse into the formation. During this process we define a maximum allowable velocity at which the sand grains will not move. Since at this step the volume is changed, the force exerted on the proppant bed is a function of the width of the fracture.

The second step of simulation considers the condition at which the rock has reached equilibrium at formation pressure. As of this point as long as the fluid drag force is less than the critical drag force the proppant bed does not move and the width remains constant.

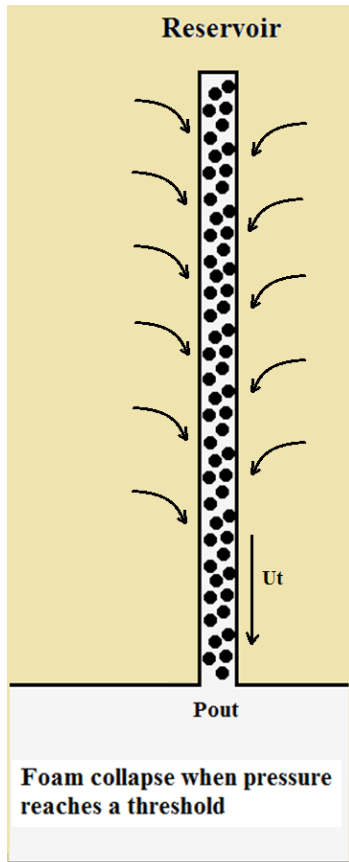


**Figure II-4:** Model of a vertical fracture with parallel planes divided by thickness of  $h$  and area of  $A$

## II.6. Results

We start modeling by evaluating constitutional equations for two phase flow. There are different approaches to evaluate two phase flow in porous media. Commonly saturation of water is assumed as one of the known variable. To use fractional flow model, it would be ideal to have total velocity as the other variable. However its evaluation depends on our gas properties which are unknown variables. One common method is to use water flowrate along with the saturation as the canonical variables. However, this approach when using for saturations near connate water saturation will fail. So instead of water flowrate we have used pressure drop as the other canonical variable. In this approach one can evaluate water permeability directly from water saturation. Then water flowrate can be determined using water permeability and pressure drop. Then using pressure drop foam texture can be evaluated. Finally, gas velocity and fractional flow can be determined using updated gas physical properties.

### Evaluating the model for fractional flow analysis:

Figures II-5 to II-8 show profiles of fractional flow ( $f_w$ ), total velocity ( $u_t$ ), apparent gas viscosity and gas velocity as a function of pressure drop and saturation. With the fractional flow, the figure is drawn between connate water saturation (0.04) and  $S_w = 0.5$ . Between the connate saturation at 0.04 and critical saturation for foam formation (0.0585) liquid fractional flow is nearly zero and gas apparent viscosity is equal to the no-foam gas viscosity. Gas velocity profile in Figure II-10 shows that below critical saturation the only way to reach to pressure drops as high as 5 psi/ft is to increase gas velocity to a significant value of 0.01 m/s. When saturation is above the critical saturation, Figure II-7 shows that at saturations near 0.1 and fractional flow of 0.1 high pressure drop of 5 psi/ft is achieved which can be attributed to the foam formation.

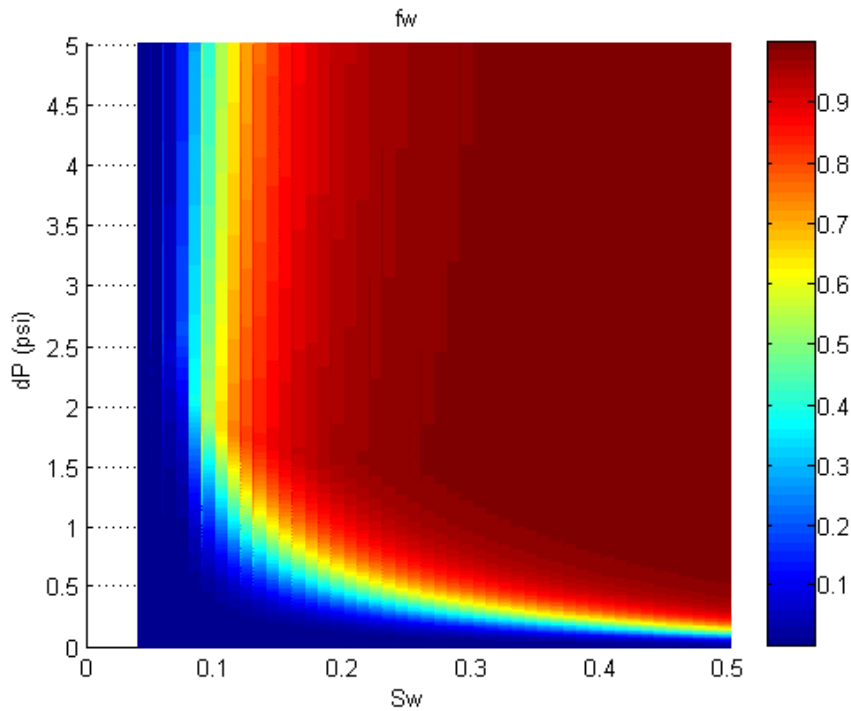


**Figure II-5:** Fractional flow as a function of saturation and pressure drop in 1 ft calculated by the proposed method

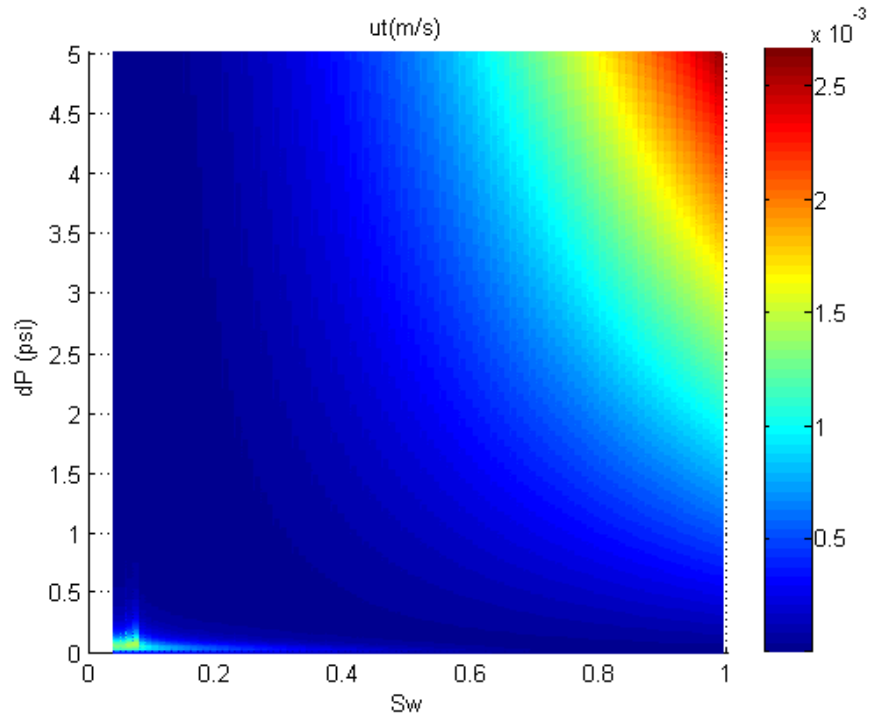


**Figure II-6:** Total velocity as a function of saturation and pressure drop in 1 ft calculated by the proposed method

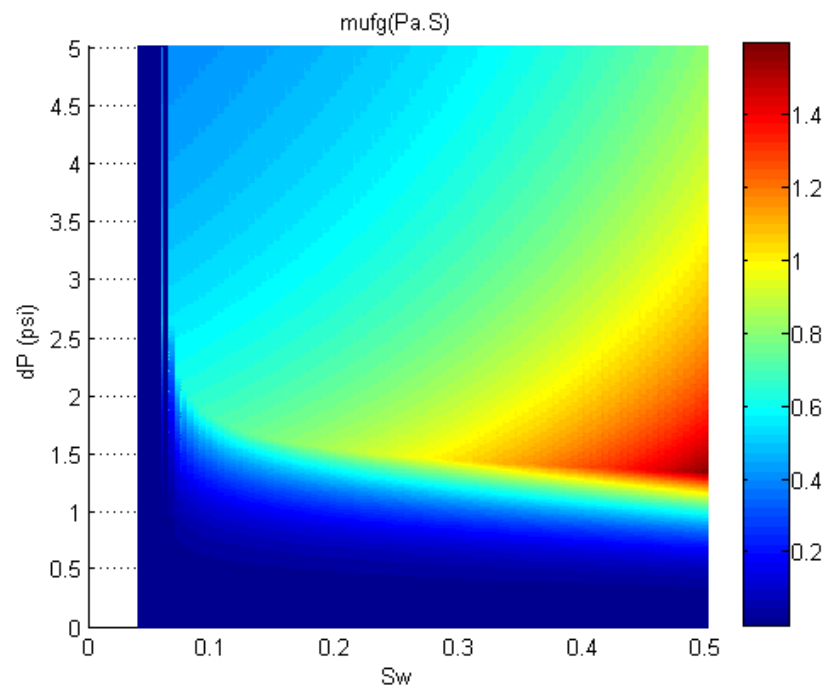


**Figure II-7:** Flowing gas viscosity as a function of saturation and pressure drop in 1 ft calculated by the proposed method

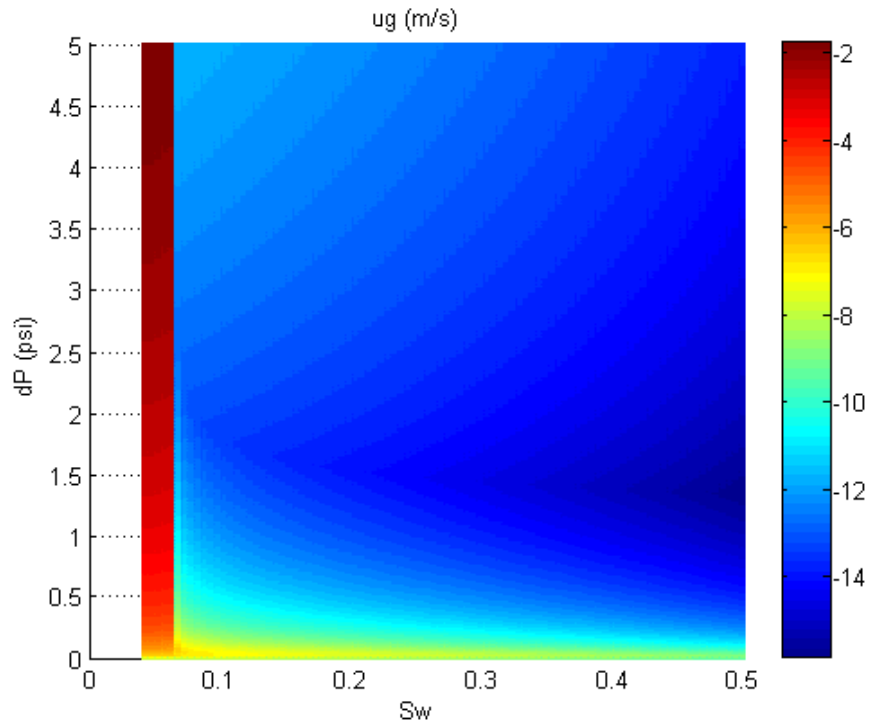


**Figure II-8:** Gas velocity calculated at fixed saturation and pressure drop per unit ft.

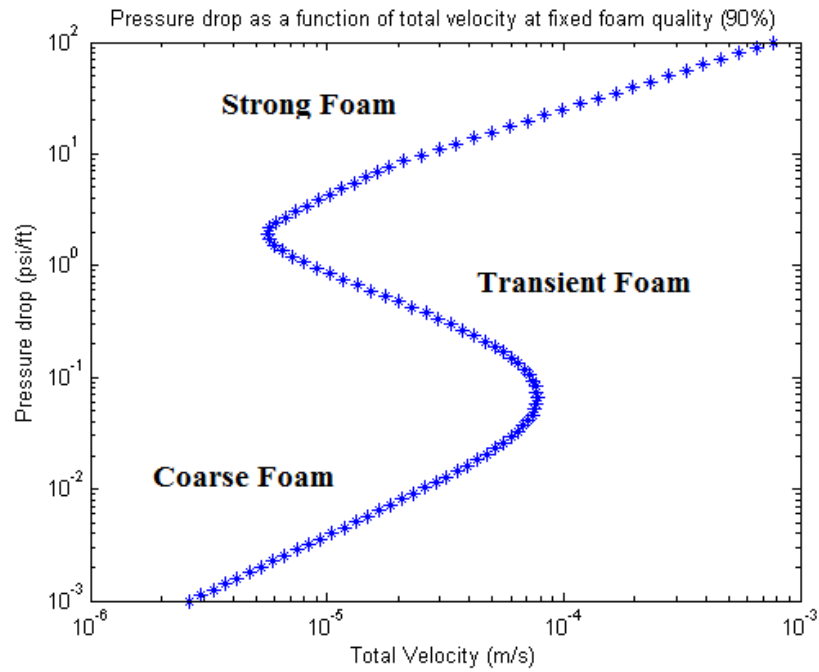


**Figure II-9:** S-curve, characteristic curve representing change in the type of foam from coarse to intermediate (transient) and strong foam.

It is favorable to report pressure drop data as a function of total velocity at fixed foam quality, since this exactly mimics the way that experimental data are collected. Pressure drop readings are collected at constant total flow rates and foam qualities. To construct our figure, we used our proposed algorithm to calculate the fractional flow for a given value of pressure drop and saturation and iteratively corrected the value of saturation to reach to the desired fractional flow. The results are shown in Figure II-9. This characteristic S-curve shows regions of different foams, lower part is the coarse foam, then there is a transition region at which when total velocity reduces the pressure drop increases and finally the strong foam region where pressure drops as high as 100 psi/ft appear.

Another characteristic curve is suggested by the previous authors to determine change in the foam regime from coarse to intermediate and then strong by drawing pressure drop as a function of gas flowrate at constant liquid flowrate. Figure II-10 shows changes in the foam regime for the liquid velocity of 1 ft/day.

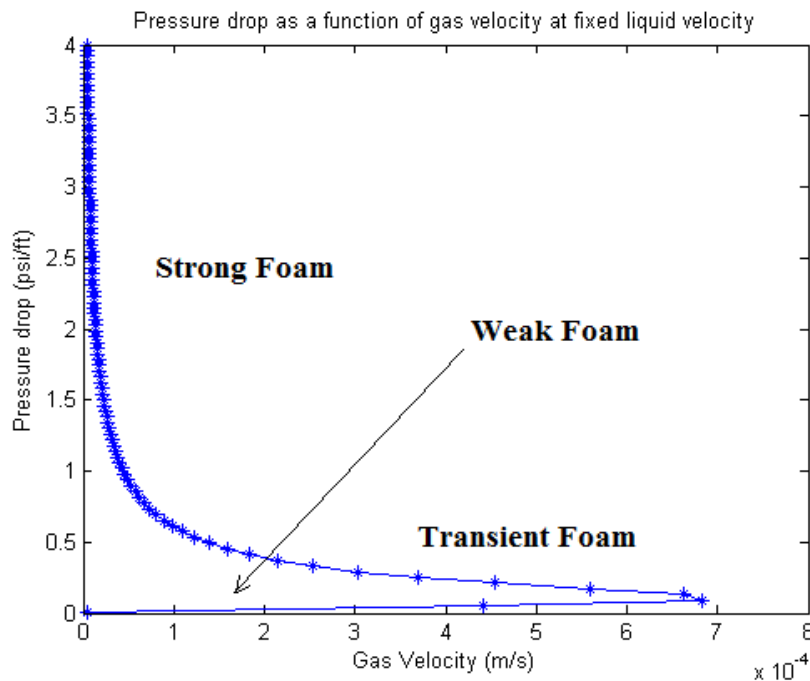


**Figure II-10:** Characteristic curve for the foam system described in this work, Pressure drop (psi/ft) as a function of gas velocity at constant liquid velocity, 1 ft/day.

### Effect of gas injection of foam quality:

During our lab tests of foam transport in bead pack and core flood experiments we observed a particular difference between high and intermediate quality foams. In a typical experiment the foam with specific quality and at a constant total flow rate was produced. When the system reached steady-state the liquid pump was shut off and gas flow rate was increased to

keep total flowrate constant. For high quality foams ( $f \sim 0.85$ ) as expected after turning off the liquid source the foam broke and pressure drop reduced. However, for low quality foams ( $f \sim 0.55$ ) once pure gas was injected into the system a rise was observed in the pressure drop and then the pressure drop reduced to a low value signaling foam breakage. Here we simulate this process for foams with high and low qualities. To address this problem we take the bead pack or core as a single grid and one dimensional fractional flow model, where evolution of saturation with time can be calculated based on the saturation value at previous time and fractional flows at inlet and outlet. One dimensional fractional flow model can be simplified as

$$\frac{\Delta S}{\Delta t} + \frac{u_t \Delta f}{\phi \Delta x} = 0$$

By discretization fractional flow equation in space and time

$$\frac{S^{t+1} - S^t}{\Delta t} + \frac{u_t f_{out} - f_{in}}{\phi \Delta x} = 0$$

At initial condition the value of saturation is known. Also as the boundary condition the fractional flow at the inlet is equal to zero, since water pump is turned off and only gas is being injected into the system. At any given moment the fractional flow in the outlet is calculated from the saturation and total velocity. Then iteratively saturation is updated as a function of time.

#### **Future work:**

In the next step of this research, using the pressure drop models we developed here we model flow of foam inside sand bed during flowback to determine improvement in the productivity of the reservoir. In addition, to understand the effect of nanoparticle to stabilize foams and determine their optimum concentration, we use experimental data and fit on our models.

#### **References**

- Aronson, A. S., Bergeron, V., Fagan, M. E., Radke, C. J., 1994. The influence of disjoining pressure on foam stability and flow in porous media. *Colloids Surface A: Physicochemical and Engineering Aspects* 83, 109.
- Dholkawala, Z. F., 2006. Application of fractional flow theory to foams in porous media. Master's Thesis, The University of Adelaide, Australia.
- Falls, A. H., Hirasaki, G. J., Patzek, T. W., Gauglitz, P. A., Miller, D. D., Ratulowski, J., 1988. Development of a mechanistic foam simulator: The population balance and generation by snap-Off. *SPE Reservoir Engineering*, 884–892 (August).

Hirasaki, G. J., Lawson, J. B., 1985. Mechanisms of foam flow through porous media – apparent viscosity in smooth capillaries. *SPE Journal*, 176–190 (April).

Kam, S. I., Nguyen, Q. P., Rossen, W. R., 2007. Dynamic simulations with an improved model for foam generation. *SPE Journal* , 35-48 (March).

Lake, L., 1989. *Enhanced oil recovery*. Prentice Hall, Englewood Cliffs, New Jersey